Construction of a molybdenum and copper co-doped nickel phosphide with lattice distortion for highly efficient electrochemical water splitting

Jiefei Li[a], Zehao Zhang [a], Xueqiong Zhang [a], Linjie Xu [a], Songyuan Yuan[a], Hang Wei[a*], Haibin Chu [a*],

[a] College of Chemistry and Chemical Engineering, Inner Mongolia Engineering and Technology Research Center for Catalytic Conversion and Utilization of Carbon Resource Molecules, Inner Mongolia University, Hohhot 010021, China. E-mail: weihang@imu.edu.cn

E-mail: chuhb@imu.edu.cn

Experimental Section

Materials

Ni foam (thickness of 1.0 mm) was purchased from Jiashide Foam Metal Co., Ltd., Suzhou. Acetone (99.9%), ethanol (99.9%), HCl (37%), $NiCl_2 \cdot 6H_2O$, $Cu(NO_3)_2 \cdot 3H_2O$, $(NH_4)_6Mo_7O_{24} \cdot 4H_2O$, urea, and NH_4F were purchased from Sinopharm Group Co., Ltd. Pt/C (20 wt %) and Nafion (5 wt %) were purchased from Johnson Matthey. RuO_2 was purchased from Sigma-Aldrich.

Pretreatment of Ni foam

Nickel foam (2.0 cm×2.4 cm×0.1 cm) was ultrasonically cleaned with 3 M HCl solution for 30 min, and subsequently rinsed with acetone, ethanol, and deionized water three times to remove the nickel oxides on the surface.

Preparation of Mo,Cu-Ni(OH)$_2$@NF, Mo-Ni(OH)$_2$@NF, Cu-Ni(OH)$_2$@NF, and Ni(OH)$_2$@NF

The in-situ growth of Mo,Cu-Ni(OH)$_2$@NF was accomplished through the one-step hydrothermal reaction, in which pretreated Ni foam and a mixed solution of $NiCl_2 \cdot 6H_2O$ (0.265 g), $Cu(NO_3)_2 \cdot 3H_2O$ (0.096 g), $(NH_4)_6Mo_7O_{24} \cdot 4H_2O$ (0.071 g), urea (0.48 g), and NH_4F (0.22 g) in 30 mL of deionized water were transferred to a Teflon-lined stainless steel reactor and heated at 120°C for 10 h, then vacuum dried via a freeze-drying method. At last, we could obtain Mo, Cu-Ni(OH)$_2$@NF flexible electrode. For comparison, Mo-Ni(OH)$_2$@NF, Cu-Ni(OH)$_2$@NF, and Ni(OH)$_2$@NF were prepared following the same procedures except using the different metal precursors.

Preparation of Mo,Cu-Ni$_2$P@NF, Mo-Ni$_2$P@NF, Cu-Ni$_2$P@NF, and Ni$_2$P@NF

To prepare the Mo,Cu-Ni$_2$P@NF, a low-temperature phosphorization method was employed here. A certain amount of NaH_2PO_2 and the as-prepared Mo,Cu-Ni(OH)$_2$@NF were placed in two quartz boats individually, and then placed in two separate positions within the tube furnace. Afterward, the samples were heated at 350 °C for 3 h with a heating rate of 2 °C min^{-1} under Ar flow atmosphere. Mo,Cu-Ni$_2$P@NF was obtained after cooled to room temperature. For comparison, Mo-Ni$_2$P@NF, Cu-Ni$_2$P@NF, and Ni$_2$P@NF were prepared following the same

procedures.

Electrochemical measurements

All the electrochemical measurements were performed on CHI 760 electrochemistry workstation. The working electrode was a Ni foam modified by catalyst (1 cm×1 cm), saturated calomel electrode and graphite rod were used as the reference and counter electrode, respectively. The polarization curves were obtained using linear sweep voltammetry (LSV) for HER and OER in 1.0 M KOH solution (pH =14) at the scanning rate of 5 mV/s. The Tafel plots were derived from the OER and HER polarization curves (2 mV/s) and constructed by the Tafel equation. The chronopotentiometric (CP) measurements were conducted to evaluate their durability. Electrochemical impedance spectra (EIS) were obtained in the frequency from 1 M Hz to 0.01 Hz in the 1.0 M KOH. The electrochemically active surface area (ECSA) can be calculated through the electrochemical double-layer capacitance (C_{dl}) with cyclic voltammetry (CV) plots in a non-Faradaic region. The CV curves were got with different scan rates (20, 40, 60, 80, and 100 mV/s) in the potential range (0.7-0.27 V versus RHE) for HER and (1.00 -1.20 V versus RHE) for OER to calculate C_{dl}. The plot of diverse scan rates versus the corresponding current density (j) between the anode and cathode ($j = j_{anodic} - j_{cathodic})/2$ can estimate the C_{dl} by their linear slope. The electrocatalytic performances for overall water splitting were measured by employing prepared catalysts as working electrodes for both OER and HER. The RuO_2 and Pt/C catalysts were used as the baseline catalysts for all the electrochemical measurements. All the potentials exhibited in this paper were calculated by the Nernst equation:$E_{RHE} = E_{SCE} + 0.242\ V \times 0.059\ pH$.

Catalyst characterizations

The Powder X-ray diffraction (XRD) patterns were performed on PANalytical Empyrean diffractometer operated at 40 kV and 40 mA using Cu Kα radiation. X-ray photoelectron spectroscopy (XPS) analysis was operated on a THS-103X spectrometer equipped with an Al Kα X-ray source (1486.6 eV). Transmission electron microscopy (TEM) characterization was acquired on a FEI Tecnai F20 system with an accelerating voltage of 200 kV. The size and morphology of the

catalysts were observed by Field Emission Scanning Electron Microscopy (FE-SEM) (Hitachi, Models-4800).

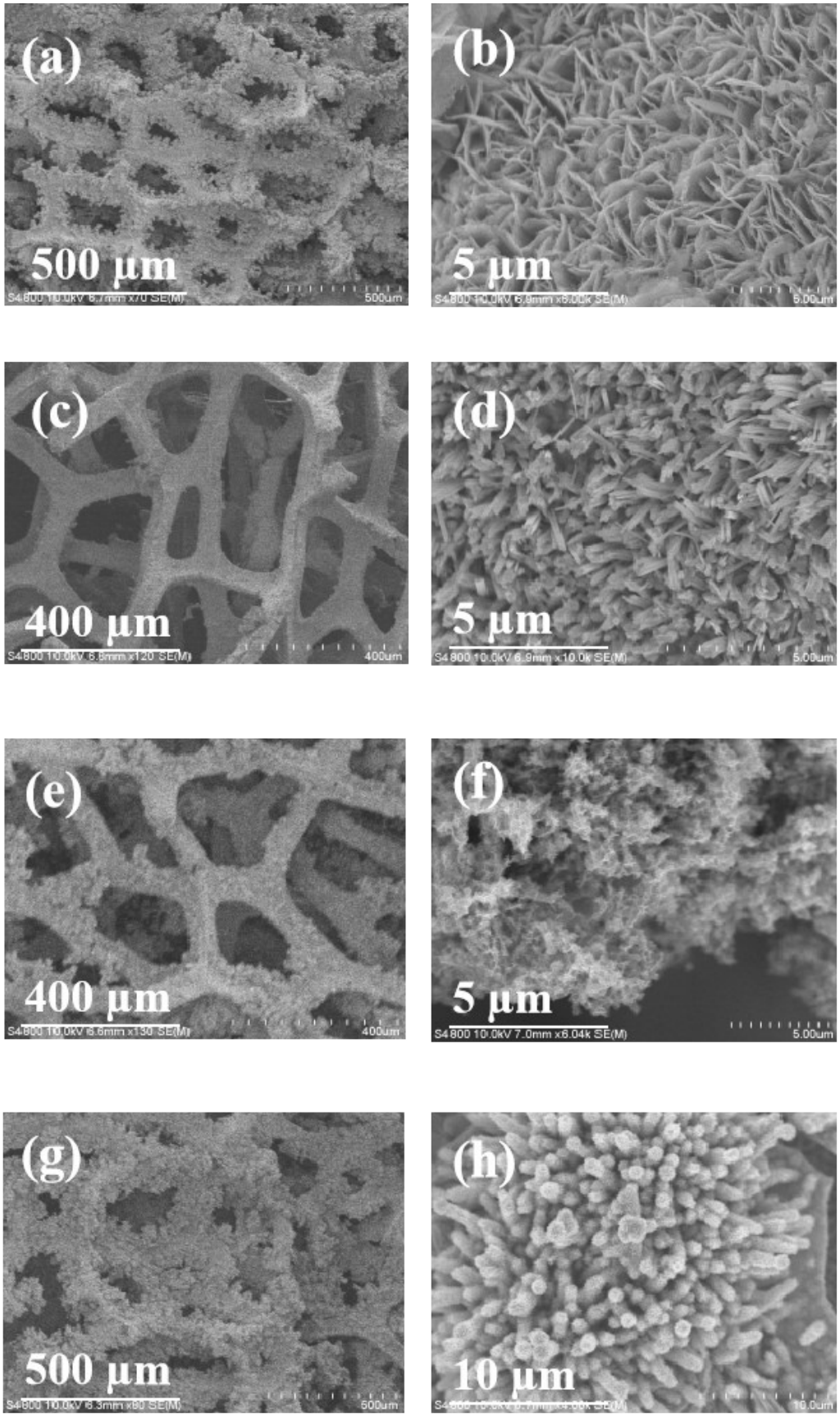

Fig.S1 SEM images of (a,b) Ni_2P@NF, (c,d) Mo-Ni_2P@NF, (e,f) Cu-Ni_2P@NF, (g,h) Mo,Cu-Ni_2P@NF.

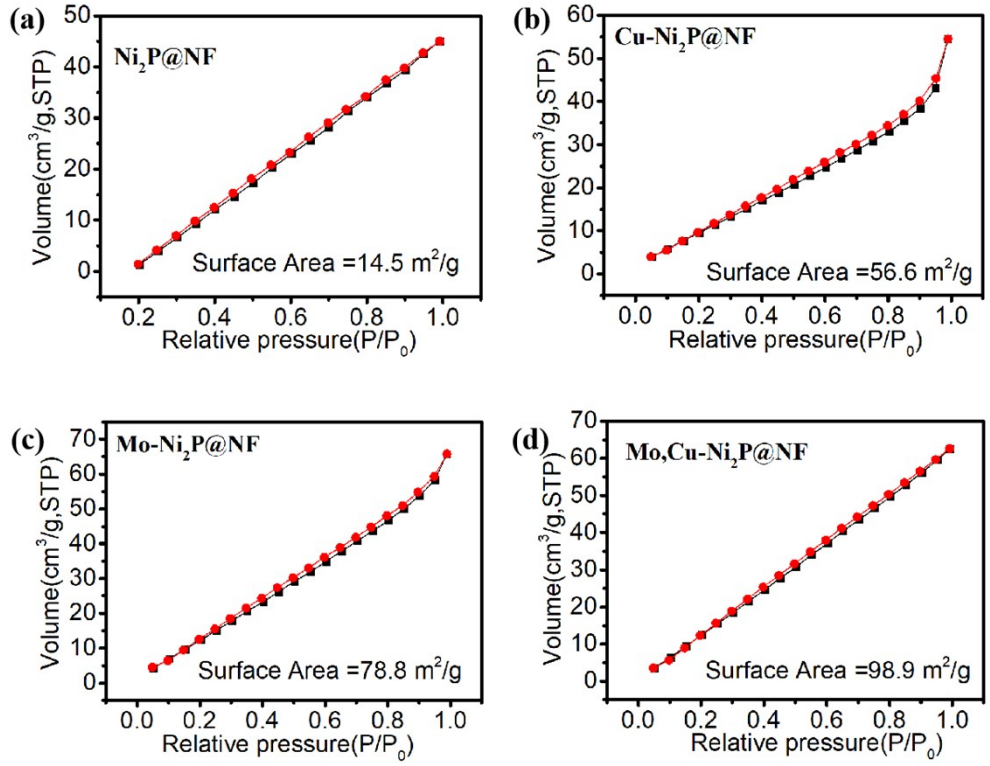

Fig.S2 The N_2 adsorption-desorption isotherm curves of Ni_2P@NF, Cu-Ni_2P@NF, Mo-Ni_2P@NF, and Mo,Cu-Ni_2P@NF.

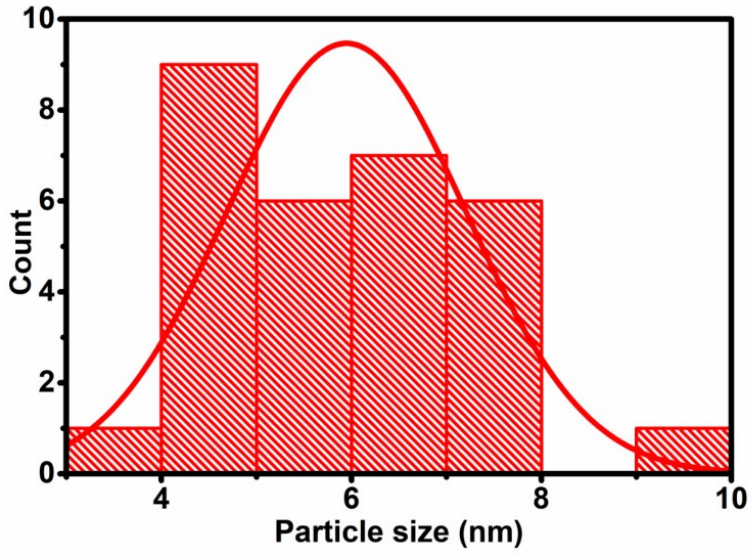

Fig.S3 Particle diameter distributions of Mo,Cu-Ni_2P nanoparticles.

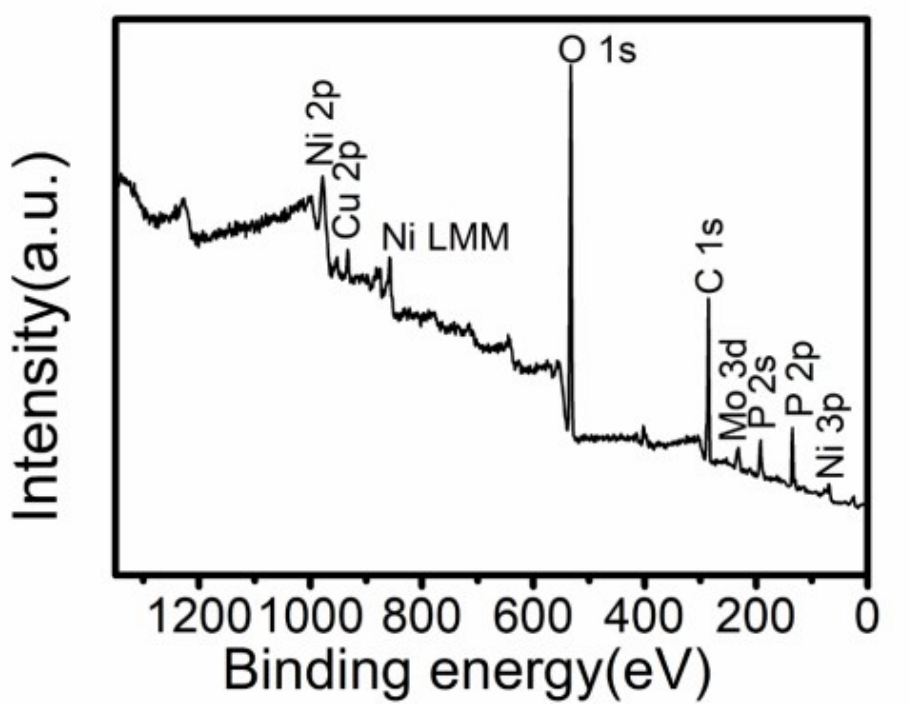

Fig.S4 The XPS spectrum of Mo,Cu-Ni_2P@NF.

Table S1 Valence analysis results derived from XPS spectra of the as-prepared electrocatalyst.

Sample	$Ni^{\delta+}$ (%)	$P^{\delta+}$ (%)	Mo^{6+} (%)	Cu^{+} (%)
Ni_2P@NF	33.3	38.4	-	
Cu-Ni_2P@NF	19.2	22.7	-	70.8
Mo-Ni_2P@NF	10.6	10.8	21.8	
Mo,Cu-Ni_2P@NF	8.95	9.3	35.7	100

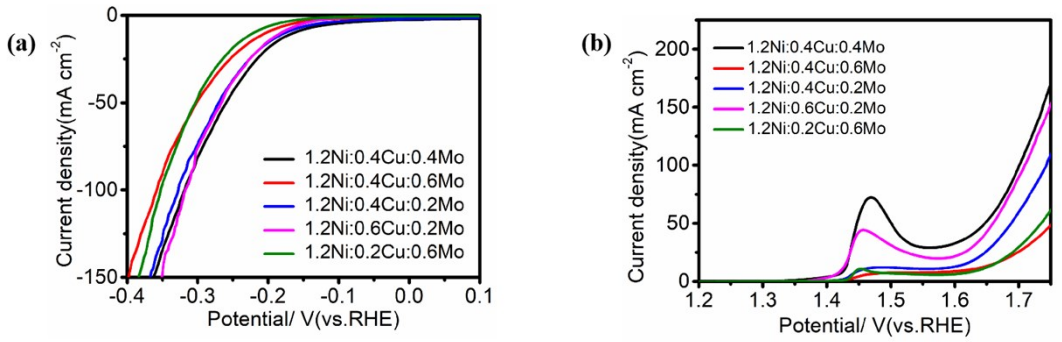

Fig. S5 HER and OER polarization curves of Mo,Cu-Ni_2P@NF with different Mo,Cu stoichiometry.

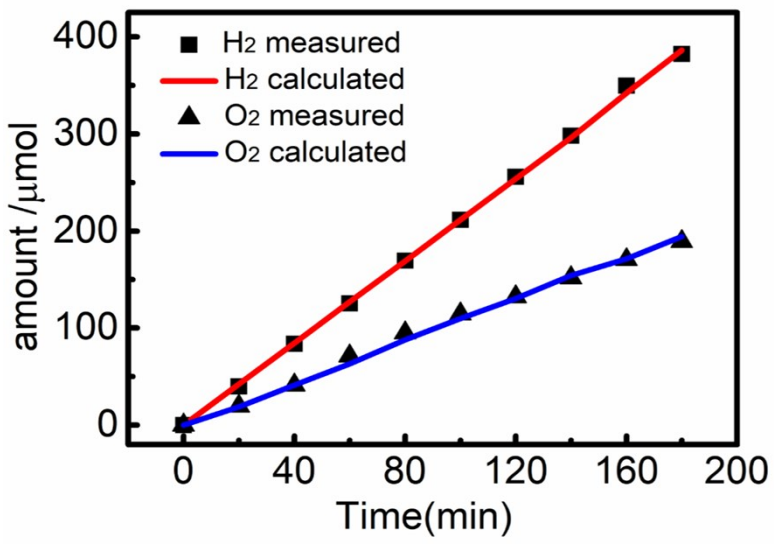

Fig. S6 The amount of H_2 and O_2 (theoretically calculated and experimentally measured) vs. time for hydrogen evolution reaction and oxygen evolution reaction.

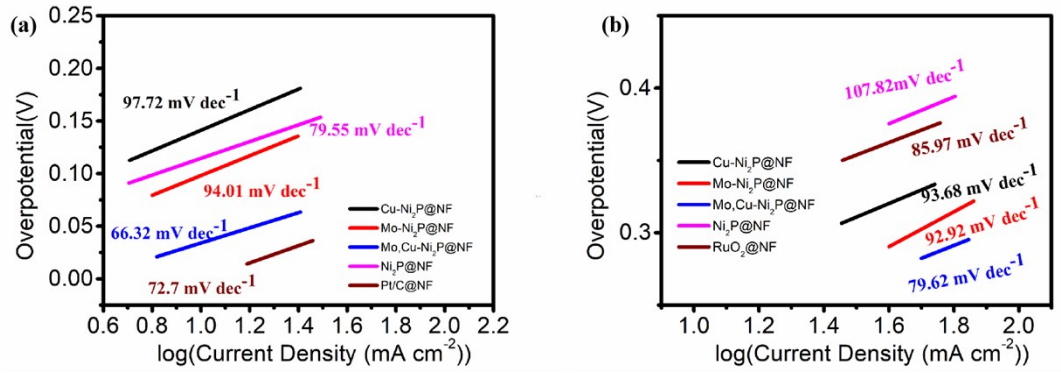

Fig. S7 Tafel plots of Ni_2P, Cu-Ni_2P, Mo-Ni_2P, Mo,Cu-Ni_2P, Pt/C, and RuO_2 in HER (a) and OER (b) process in 1.0 M KOH.

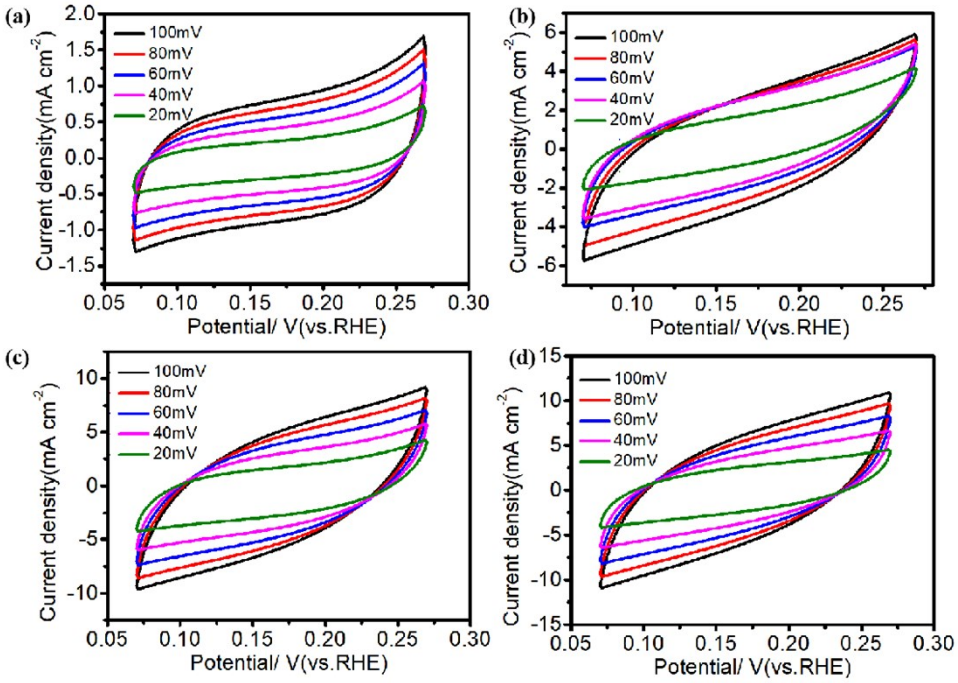

Fig. S8 Cyclic voltammograms of (a) Ni_2P, (b) Cu-Ni_2P, (c) Mo-Ni_2P, and (d) Mo,Cu-Ni_2P, measured in a potential window without Faradaic process at different scan rates: 20, 40, 60,80 and 100 mV s^{-1} in the potential range of 1.00 V to 1.20 V vs RHE.

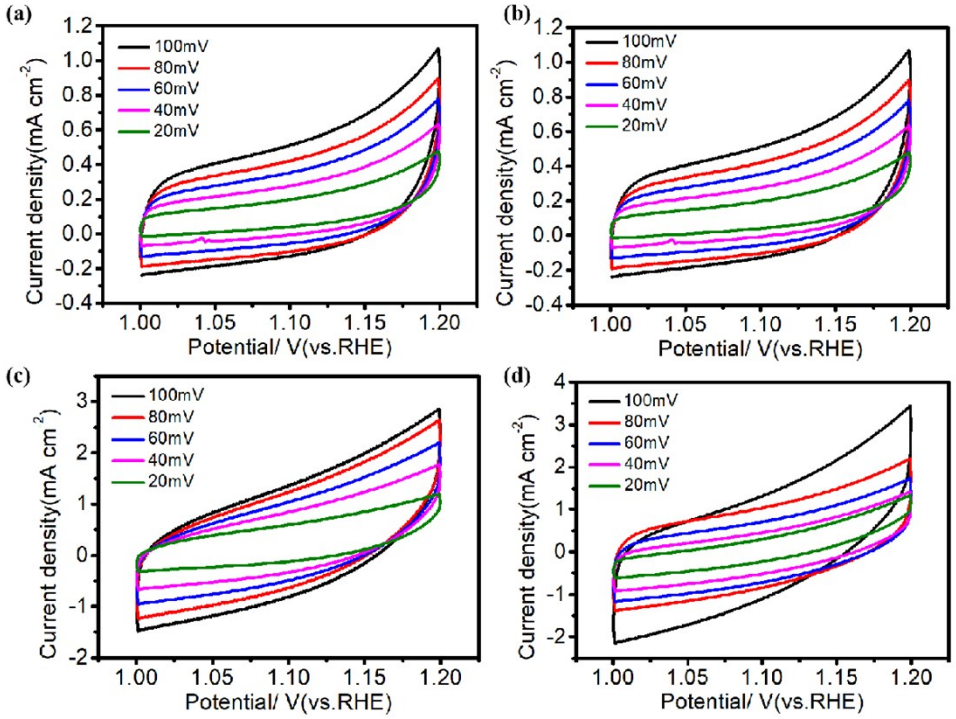

Fig. S9 Cyclic voltammograms of (a) Ni_2P, (b) Cu-Ni_2P, (c) Mo-Ni_2P, and (d) Mo,Cu-Ni_2P, measured in a potential window without Faradaic process at different scan rates: 20, 40, 60,80 and 100 mV s^{-1} in the potential range of 1.00 V to 1.20 V vs RHE.

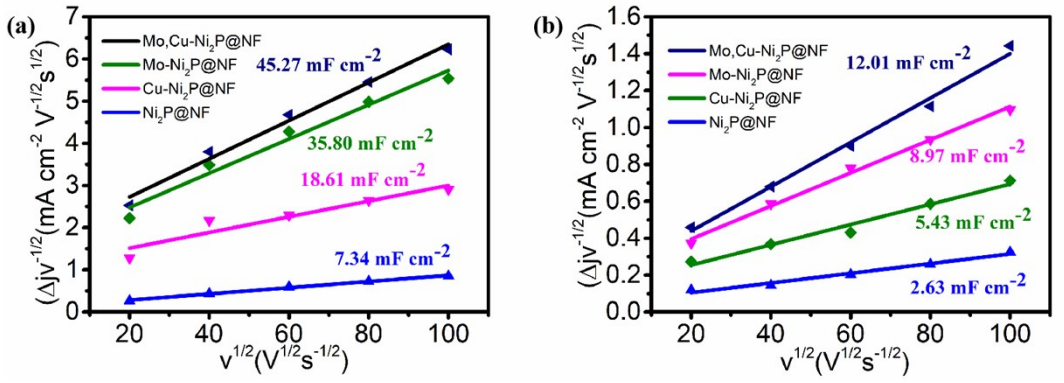

Fig. S10 The double-layer capacitance of Ni_2P, Cu-Ni_2P, Mo -Ni_2P, and Mo,Cu-Ni_2P in HER (a) and OER (b) process in 1.0 M KOH.

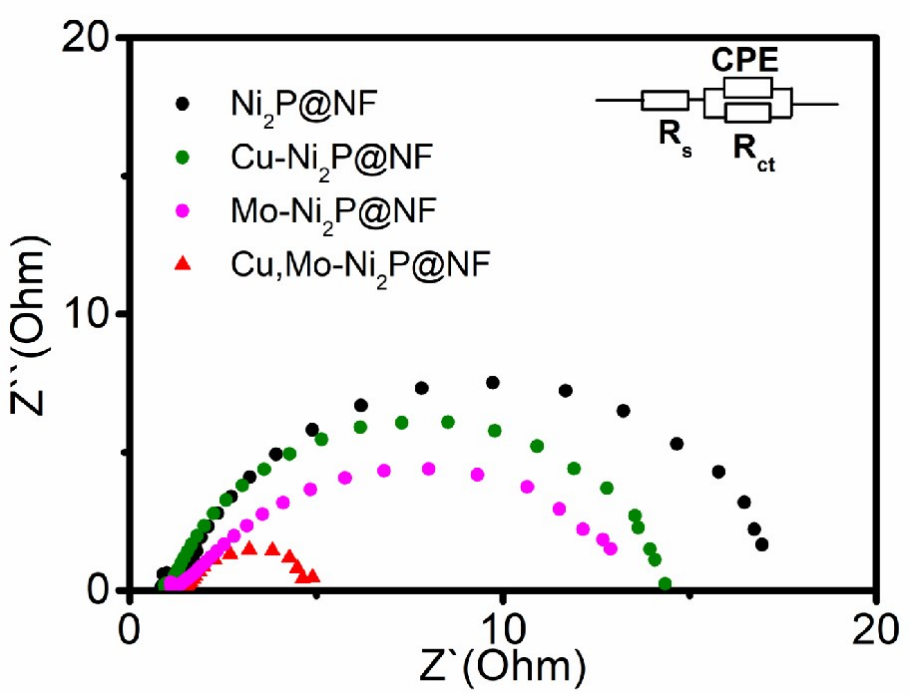

Fig. S11 Nyquist plots of Ni_2P@NF, Cu-Ni_2P@NF, Mo-Ni_2P@NF, and Mo,Cu-Ni_2P@NF.

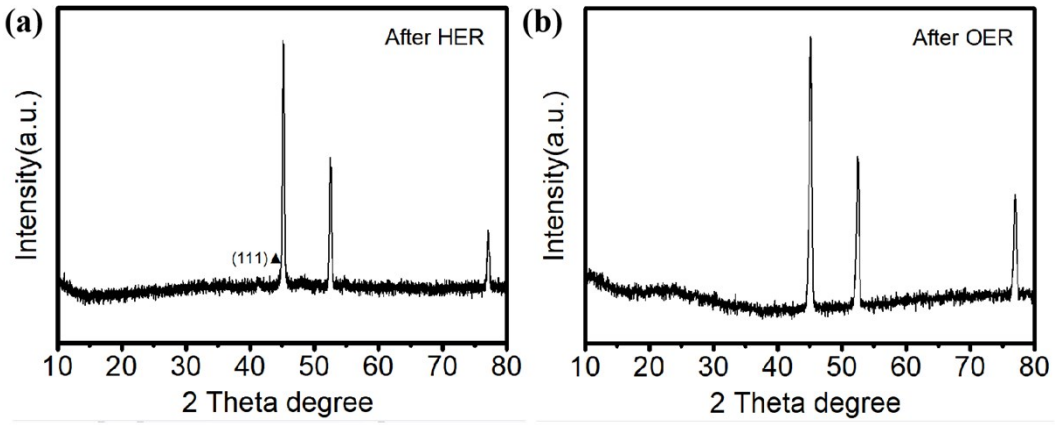

Fig. S12 XRD spectra of Mo,Cu-Ni_2P@NF after stability testing.

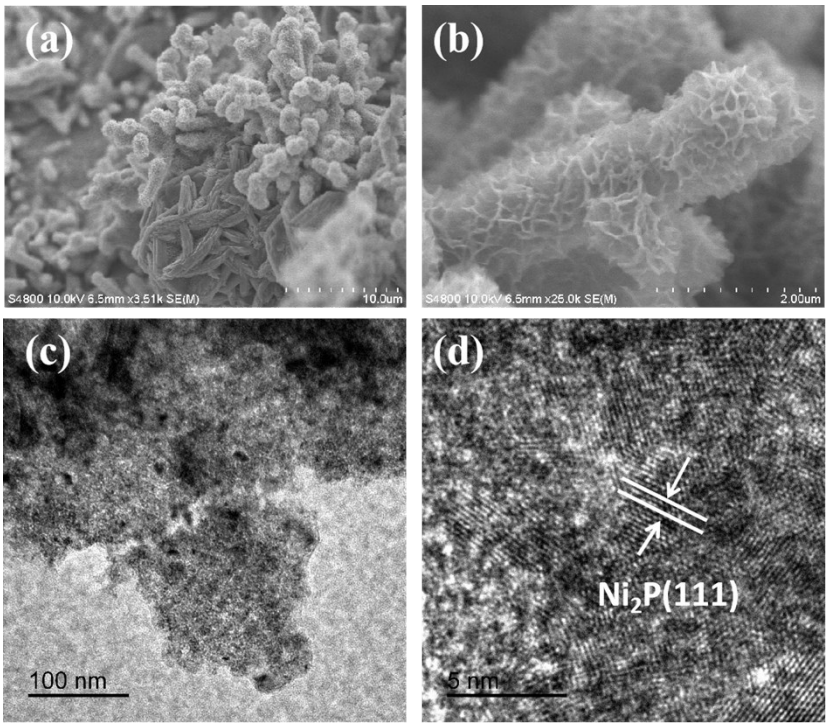

Fig. S13. (a) SEM and (b)TEM images of Mo,Cu-Ni_2P@NF after 20 h HER stability testing.

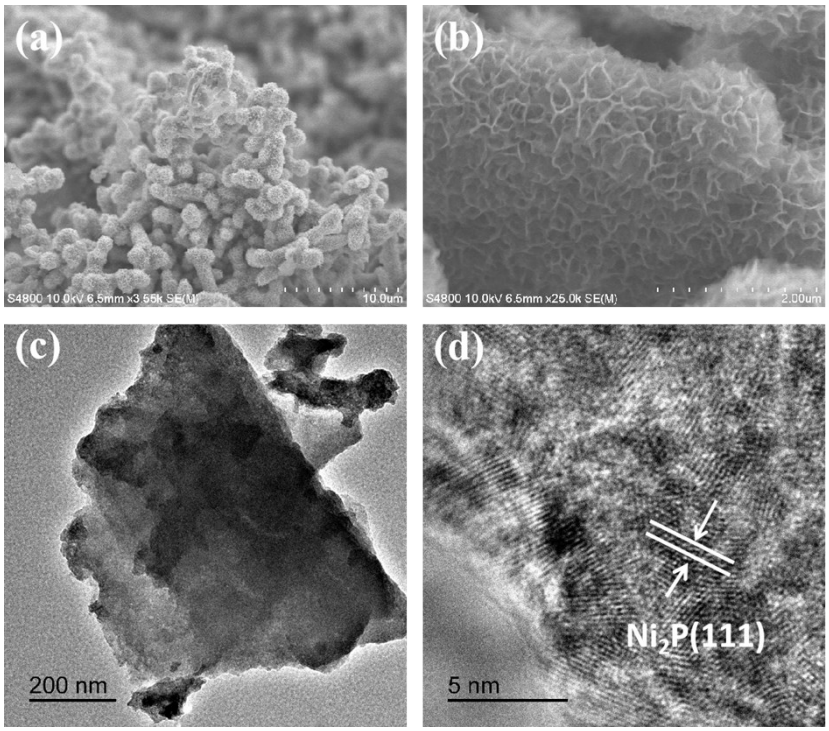

Fig. S14. (a) SEM and (b)TEM images of Mo,Cu-Ni_2P@NF after 20 h OER stability testing.

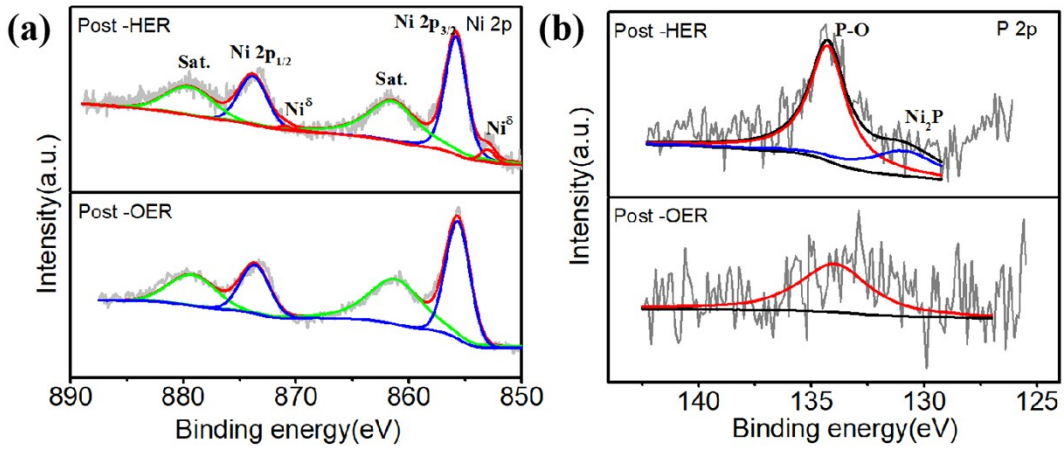

Fig. S15 XPS spectra of Mo,Cu-Ni_2P@NF after stability testing.

Table S2. Comparison of recent nickel-based electrocatalysts for HER in alkaline electrolytes.

Catalysts	Electrolyte	Overpotential (η)	Current density (i_0)	Tafel slope (b)	Ref
Mo,Cu-Ni_2P@NF	1 M KOH	34 mV	10 mA cm^{-2}	66.32 mV dec^{-1}	This work
NiP/NF	1 M KOH	102 mV	10 mA cm^{-2}	90 mV dec^{-1}	[1]
$NiP_{0.62}S_{0.38}$	1 M KOH	52 mV	10 mA cm^{-2}	52.3 mV dec^{-1}	[2]
$Ni_{90}P_{10}$/Ti	1 M KOH	212 mV	10 mA cm^{-2}	75.4 mV dec^{-1}	[3]
Ni-P/CF	1 M KOH	98 mV	10 mA cm^{-2}	55 mV dec^{-1}	[4]
Mo–Ni_2P nanowires	1 M KOH	78 mV	10 mA cm^{-2}	109 mV dec^{-1}	[5]
Ni/Ni_8P_3	1 M KOH	130mV	10 mA cm^{-2}	58.5 mV dec^{-1}	[6]
Ni/NiS	1 M KOH	230mV	10 mA cm^{-2}	123.3 mV dec^{-1}	[6]
Ni_2P/Ni_3S_2 HNAs nanoflakes	1 M KOH	80 mV	10 mA cm^{-2}	65 mV dec^{-1}	[7]
Ni_2P/MoO_2@MoS_2	1 M KOH	159mV	10 mA cm^{-2}	77 mV dec^{-1}	[8]
Ni–Co–P/NF	1 M KOH	160mV	10 mA cm^{-2}	108mV dec −1	[10]
P/$Ni(OH)_2$/$NiMoO_4$	1 M KOH	60 mV	10 mA cm^{-2}	130 mV dec^{-1}	[11]
NiCoFe phosphate NSs-C/NF	1 M KOH	231 mV	10 mA cm^{-2}	86 mV dec^{-1}	[12]
Ni_2P/rGO	1 M KOH	142 mV	10 mA cm^{-2}	58 mV dec^{-1}	[13]
NiP/NiFeP/C	1 M KOH	87 mV	10 mA cm^{-2}	38mV dec^{-1}	[14]

NiP_2−Fe-2	1 M KOH	86 mV	10 mA cm^{-2}	63.1 mV dec^{-1}	[15]
NFNS@NiP@Plate,	1 M KOH	243 mV	10 mA cm^{-2}	141 mV dec^{-1}	[16]
NiFeCoP/NM	1 M KOH	33 mV	10 mA cm^{-2}	71.1 mV dec^{-1}	[17]

Table S3. Comparison of recent nickel-based electrocatalysts for OER in alkaline electrolytes.

Catalysts	**Electrolyte**	**Overpotential (η)**	**Current density (i_0)**	**Tafel slope (b)**	**Ref**
Mo,Cu-Ni_2P@NF	1 M KOH	341 mV	100 mA cm^{-2}	79.62 mV dec^{-1}	This work
NiP/NF	1 M KOH	320 mV	10 mA cm^{-2}	78 mV dec^{-1}	[1]
$NiP_{0.62}S_{0.38}$	1 M KOH	270 mV	10 mA cm^{-2}	-	[2]
Ni-P/CF	1 M KOH	325 mV	10 mA cm^{-2}	120 mV dec^{-1}	[4]
Ni/Ni_8P_3	1 M KOH	270 mV	10 mA cm^{-2}	73.2 mV dec^{-1}	[6]
Ni/NiS	1 M KOH	340 mV	10 mA cm^{-2}	109.8 mV dec^{-1}	[6]
Ni_2P/Ni_3S_2 HNAs nanoflakes	1 M KOH	240 mV	10 mA cm^{-2}	62 mV dec^{-1}	[7]
Ni_2P/MoO_2@MoS_2	1 M KOH	280 mV	10 mA cm^{-2}	85 mV dec^{-1}	[8]
Ni–Co–P/NF	1 M KOH	350 mV	20 mA cm^{-2}	324.6 mV dec^{-1}	[10]
$P/Ni(OH)_2/NiMoO_4$	1 M KOH	270 mV	10 mA cm^{-2}	-	[12]
NiCoFe phosphate NSs-C/NF	1 M KOH	240 mV	10 mA cm^{-2}	58 mV dec^{-1}	[13]
Ni_2P/rGO	1 M KOH	260 mV	10 mA cm^{-2}	62 mV dec^{-1}	[14]
NiP/NiFeP/C	1 M KOH	300 mV	10 mA cm^{-2}	81 mV dec^{-1}	[15]
NFNS@NiP@Plate,	1 M KOH	197 mV	10 mA cm^{-2}	51 mV dec^{-1}	[16]
NiFeCoP/NM	1 M KOH	277 mV	10 mA cm^{-2}	48.9 mV dec^{-1}	[17]
$Ni_2P_2O_7 \cdot 8H_2O$/SS	1 M KOH	239 mV	10 mA cm^{-2}	51.5 mV dec^{-1}	[18]
Ni_2P/VP_2/NF	1 M KOH	220 mV	10 mA cm^{-2}	49 mV dec^{-1}	[19]

Reference:

[1] Z. Yuan, C. Chen, Z. Hu, *J. Energy Chem*. 2017, **26**, 1196.

[2] J. Luo, D. Li, F. Tian, *J. Mater. Chem.* A. 2017, **5**, 14865.

[3] C. Li, Y. Zhang, S. Lu, *Chem. Commun.* 2018, **54**, 12408.

[4] C. Li, S. Gu, Q. Liu, *J. Power Sources.* 2015, **299**, 342.

[5] Y. Sun, L. Hang, Q. Shen, *Nanoscale* 2017, **9**, 16674.

[6] F. Gao, T. Chen, M. Yi, L. Qing, *Adv. Funct. Mater.* 2016, **26**, 3314.

[7] X. Wang, Y. Liu, Y. Pan, *Nano Energy* 2018, **51**, 26.

[8] D. Zhao, H. Wang, C. Selomulya, *Nanoscale* 2017, **9**, 17349.

[9] W. Cheng, H. Zhang, Q. Liu, *J. Mater. Chem. A.* 2018, **6**, 9420.

[10] Y. Gong, J. Wang, Z. Xu, *J. Mater. Chem. A.* 2018, **6**, 12506.

[11] Y. Li, H. Tan, W. Xi, G. Yan, *Dalton Tran.* 2018, **47**, 8787.

[12] H. Lin, X. Wang, *Nanoscale* 2018, **101**, 2975.

[13] L. Yan, L. Li, X. Zhao, *J. Mater. Chem. A.* 2019, **6**,1682.

[14] Y. Yan, B. Weng, *J. Mater. Chem. A.* 2019, **7**, 7168.

[15] M. Pi, S. Chen, J. Li, *ACS Appl. Mater Interfaces.* 2019, **11**, 14059.

[16] J. Ding, E. Peng, X. Su, X. Li, *Adv. Sci.* 2019, **6**, 1801670.

[17] C. Zhao, M. Zhou, Q. Sun, Z. Wan, *Electrochim. Acta* 2019, **306**, 651.

[18] U. Patil, S. Marje, P. Katkar, *J. Alloys. Compd.* 2019, **779**, 49.

[19] H. Fu, C. Tian, X. Zhang, *Adv. Mater.* 2019, **31**, 1901174.